Soft Particles at Liquid Interfaces

Please check the document version of this publication:

• A submitted manuscript is the version of the article upon submission and before peer-review. There can be important differences between the submitted version and the official published version of record. People interested in the research are advised to contact the author for the final version of the publication, or visit the DOI to the publisher's website.
• The final author version and the galley proof are versions of the publication after peer review.
• The final published version features the final layout of the paper including the volume, issue and page numbers.

Link to publication

Soft Particles at Liquid Interfaces: From Molecular Particle Architecture to Collective Phase Behavior

Simone Ciarella, Marcel Rey, Johannes Harrer, Nicolas Holstein, Maret Ickler, Hartmut Löwen, Nicolas Vogel,* and Liesbeth M. C. Janssen*

Read Online

ACCESS | Metrics & More | Article Recommendations | Supporting Information

ABSTRACT: Soft particles such as microgels can undergo significant and anisotropic deformations when adsorbed to a liquid interface. This, in turn, leads to a complex phase behavior upon compression. To date, experimental efforts have predominantly provided phenomenological links between microgel structure and resulting interfacial behavior, while simulations have not been entirely successful in reproducing experiments or predicting the minimal requirements for the desired phase behavior. Here, we develop a multiscale framework to link the molecular particle architecture to the resulting interfacial morphology and, ultimately, to the collective interfacial phase behavior. To this end, we investigate interfacial morphologies of different poly(N-isopropylacrylamide) particle systems using phase-contrast atomic force microscopy and correlate the distinct interfacial morphology with their bulk molecular architecture. We subsequently introduce a new coarse-grained simulation method that uses augmented potentials to translate this interfacial morphology into the resulting phase behavior upon compression. The main novelty of this method is the possibility to efficiently encode multibody interactions, the effects of which are key to distinguishing between heterostructural (anisotropic collapse) and isostructural (isotropic collapse) phase transitions. Our approach allows us to qualitatively resolve existing discrepancies between experiments and simulations. Notably, we demonstrate the first in silico account of the two-dimensional isostructural transition, which is frequently found in experiments but elusive in simulations. In addition, we provide the first experimental demonstration of a heterostructural transition to a chain phase in a single-component system, which has been theoretically predicted decades ago. Overall, our multiscale framework provides a phenomenological bridge between physicochemical soft-particle characteristics at the molecular scale and nanoscale and the collective self-assembly phenomenology at the macroscale, serving as a stepping stone toward an ultimately more quantitative and predictive design approach.
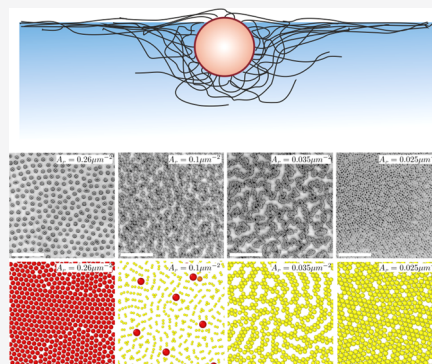
INTRODUCTION

Adsorption of colloidal particles to liquid interfaces is ubiquitous and relevant in both fundamental science and technological applications.[1−3] For example, in functional soft matter applications, the presence of adsorbed particles imparts kinetic stability of emulsions,[4,5] liquid marbles,[6,7] and foams.[8,9] Additionally, colloidal particles can serve as masks to obtain complex nanoscale surface patterns.[10−13] Furthermore, since liquid interfaces confine the particles on two dimensions, they serve as ideal templates for fundamental studies of colloidal interaction, crystallization, and self-assembly.[1,3,14]

At liquid interfaces, colloidal particles are able to self-assemble into ordered two-dimensional (2D) crystals.[15] Depending on the balance between attractive capillary and van der Waals forces and repulsive dipole and electrostatic forces,[3] monodisperse spherical particles typically form hexagonal close-packed or non-close-packed structures.[16] In recent years, the interfacial behavior of soft-particle systems at liquid interfaces has been attracting attention.[17] In contrast to their rigid analogues, soft particles can deform significantly and anisotropically under the

influence of surface tension[18] and may assume a characteristic core−corona morphology[19−22] to cover more interfacial area than assumed from their bulk diameter. This change in morphology leads to a more complex interfacial phase behavior. At low surface pressure Π (corresponding to a large available area per particle A_P), soft particles typically assemble into a hexagonal non-close-packed configuration in which the particle coronae are in contact.[12,17,21,23−29] Upon compression to decrease the available area at the interface, different phase behaviors may be observed: either the hexagonal phase remains intact, with a lattice constant that decreases continuously (continuous transition) or discontinuously (isostructural transition) upon compression, or a symmetry-breaking tran-
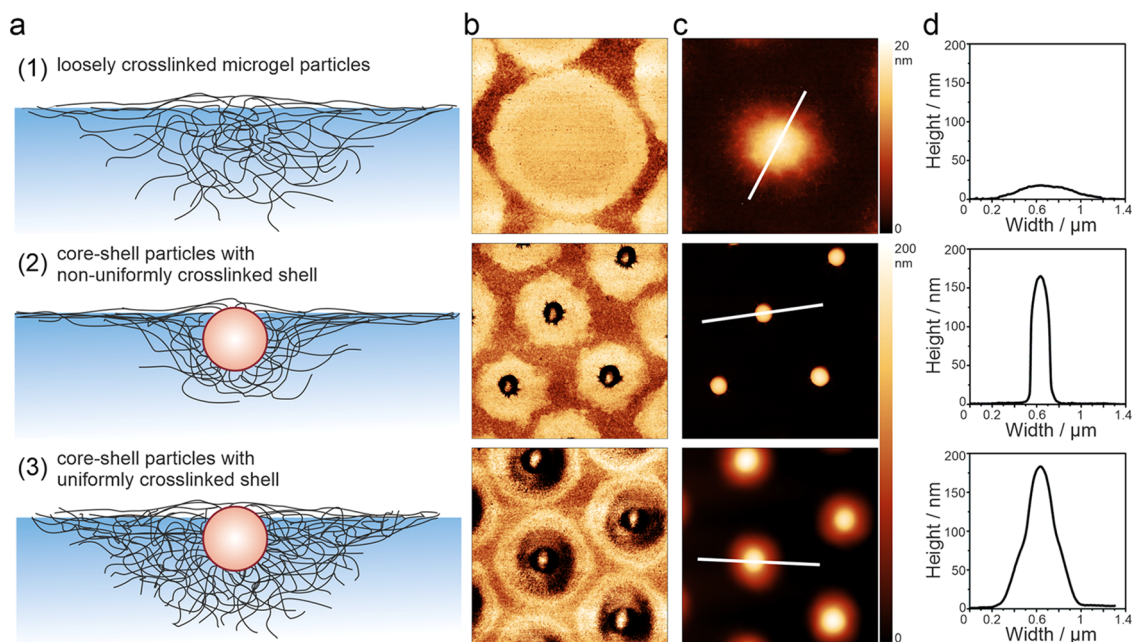
Figure 1. Molecular architecture of soft microgel systems controls their interfacial morphologies. (a) Schematic illustration of the hypothesized interfacial morphology. (b−d) Corresponding AFM phase (b) and height (c) images. Cross-section (d) measured along the white lines of (c), highlighting the difference in their interfacial morphologies. Images 2×2 μm^2.

sition occurs toward a new phase without hexagonal order. We refer to the latter as a heterostructural transition.

Despite their broad relevance, the 2D phase behavior of soft particles is still confounded by significant discrepancies between the theory and experiment. For example, the isostructural transition is experimentally among the most commonly observed behaviors,[12,21,23−28,30,31] yet in computer simulations, it has proven difficult to model a discontinuous transition between non-close-packed and close-packed hexagonal phases. Thus far, this isostructural transition could only be predicted by the simulation[32] and theory[33−35] for very short shells that do not match the experiments. Conversely, 2D heterostructural transitions toward, e.g., chain,[36−40] cluster,[41] honeycomb,[42] or quasicrystalline[42,43] phase can be simulated via relatively simple Jagla pair potentials.[36,44,45] However, to date, no experimental single-component system has exhibited such heterostructural behavior, even though the synthesized particles should, at first sight, behave according to Jagla.[36,44,45] These apparent incongruities in experiments and simulations underline the need for a more rigorous understanding of the relationship between molecular soft-particle properties, interfacial morphology, and macroscopic interfacial phase behavior.

In this work, we seek to address these discrepancies, at least on a qualitative and semiphenomenological level, by developing a multiscale-based framework for the 2D phase behavior of monodisperse soft particles. We combine experiments and a novel simulation approach to connect the collective phase behavior on the macroscale to the single-particle morphology on the nanoscale. Our framework recognizes that the emergent phase behavior ultimately stems from (anisotropic) two- and many-body interactions among particles; these interactions, in turn, must follow from the molecular architecture of each individual particle. Thus, by tailoring the morphology that the microgels assume at the liquid interface via their molecular architecture, we are able to achieve continuous, isostructural, and heterostructural 2D transitions.

RESULTS AND DISCUSSION

In the following, we consider the phenomenology of three different 2D phase behaviors of single-component soft-particle systems. First, the continuous regime corresponds to a continuous decrease in lattice spacing upon compression while preserving the overall hexagonal lattice structure. The heterostructural regime is characterized by a change in the symmetry upon compression, for example, from hexagonal to chain phases. At last, the isostructural case is characterized by a discontinuous transition that proceeds via hexagonal clusters of close-packed particles that nucleate within a non-close-packed hexagonal phase. As detailed below, our simulation approach is able to phenomenologically capture all different phase transition regimes by invoking only a small number of free parameters. In combination with experiments, this approach allows us to recognize common qualitative features among particles from the same regime and to provide hypotheses connecting the interfacial morphologies with the macroscopic phase behavior.

From Molecular Architecture to Interfacial Morphology. For our experiments, we use poly(N-isopropylacrylamide) (PNIPAM) microgels with (N,N′-methylenebisacrylamide) (BIS) as a cross-linker as a widely used model system with well-established synthesis protocols.[46] As the first particle system, we synthesize a microgel with very low cross-linking density (1 mol % BIS), as used in our previous work.[24] The second and third particle systems are silica−PNIPAM core−shell structures,[12] providing two distinct length scales, which are given by the hard silica core and the soft PNIPAM shell, respectively. We capitalize on the known difference in reactivity of the cross-linker BIS compared to the NIPAM monomer,[47,48] which leads to a cross-linking gradient from the center toward the periphery of microgels,[49] and vary the uniformity of the cross-linker distribution while keeping the overall concentration similar (5 mol % BIS). In the second particle system, we create a nonuniform cross-linking density through a batch synthesis process of the PNIPAM shell. In this case, the monomer and

cross-linker are present at the beginning of the reaction. The higher reactivity of the cross-linker means that it is more rapidly consumed in the course of the reaction. Therefore, a decrease in the cross-linking density from the core toward the periphery of the microgel shell is expected. In the third particle system, we pursue the opposite strategy and ensure a uniform cross-linking density throughout the shell by continuous feeding of the monomer and cross-linker. This feeded synthesis ensures that the ratio between both molecules remains constant throughout the course of the reaction.[12,50,51] Note that with the exception of the second particle system, all particle systems have been synthesized and used in the literature before. Here, our aim is to re-examine their interfacial behavior in the framework of our simulation method and to interpret the resulting phase transitions on the basis of their interfacial morphology and the (an)isotropy of the pressure-induced collapse.

To first connect the molecular architecture of the individual particle systems with their interfacial morphology, we assemble the particles at the air/water interface without compression (surface pressure $\Pi = 0$) and deposit them onto a solid substrate.[17] We then characterize their morphology in the dry state using atomic force microscopy (AFM) (Figure 1). Although drying will cause changes to the overall microgel dimensions, we assume that the morphology of the particle at the interface remains intact. We and others have previously shown that both the interfacial morphology and the hexagonal symmetry of the assembly phases are effectively preserved after transfer to a solid substrate and that they resemble the shape of microgels imaged directly at the interface.[17,21,23,26] This observation indicates that capillary forces are unlikely to change the microgel morphology, which is further supported by the known affinity of microgels to silica surfaces.[52] It is known that microgels deform at the air/water interface and assume a characteristic core−corona morphology, where the core consists of the more cross-linked central region of the microgel, while the corona forms as an extremely thin polymer layer, presumably by dangling polymer chains stretching out from the microgel periphery.[17,19−22] Because of its very thin nature, this corona is often not visible in scanning electron microscopy (SEM) and AFM height images but can be clearly recognized by its contrast in AFM phase images.[17]

We observe that all three particle systems expand at the liquid interface under the effect of surface tension and assume a core−corona morphology visible in the AFM height and phase images (Figure 1b,c). Although their composition and bulk dimensions are comparable (Figure S1a), the three different particle systems exhibit substantial differences in their interfacial morphology. The AFM height image of the loosely cross-linked microgels (Figure 1(1)) without the silica core displays a broad, flattened profile with a continuous and regular thinning from the center, resulting from the particle's high degree of deformability (Figure 1c, top). In addition, the AFM phase image clearly reveals a corona surrounding the central region, which is too thin to be seen in the AFM height image (Figure 1c, top). We therefore hypothesize that the shape of the microgels at the liquid interface will be similarly three-dimensional with a continuous decrease in height toward the periphery, as seen in the AFM height image. This interfacial morphology is found for different simulation approaches describing the deformation of soft particles at interfaces.[22,53] For the core−shell particles with nonuniform cross-linked shells (Figure 1(2)) we observe a well-defined core in the AFM height image with an abrupt transition to the corona, which is only visible in the AFM phase image due to its very thin

nature. We assume that the same morphology is present at the liquid interface, i.e., these particles exhibit a very flat and extended two-dimensional corona. This morphology reflects the ability of the loosely connected polymer chains at the outer periphery of the microgel shell to extend at the interface to minimize surface tension. For the core−shell particles with uniform cross-linking density (Figure 1(3)) we observe a more continuous density profile from the center to the periphery. In the AFM height image, a deformed polymeric shell surrounding the silica core is visible. The AFM phase image reveals the presence of an additional, extremely thin corona. The uniform cross-linker distribution in this sample prevents the polymer chains to fully extend at the interface. As a consequence, the shell retains an appreciable volume around the silica core, which transitions into a thin corona at the periphery away from the core. Although samples (2) and (3) have comparable interfacial dimensions, the interfacial region covered by the thin corona is much reduced in sample (3).

Augmented Potential Simulation Model. To model the phase behaviors of the three different systems in silico, we require a simulation method that can account for all of the relevant soft-particle properties but that at the same time is sufficiently computationally efficient to simulate a large collection of particles.[22,54−61] Although coarse-grained molecular dynamics (MD) simulations with simple pair potentials are already capable of predicting continuous and heterostructural transitions,[36,44,45] the 2D isostructural phase transition has not yet been captured by conventional MD methods. Here, we invoke a recently introduced, more advanced simulation method based on augmented variables,[62,63] allowing us to explicitly account for a partial or full collapse of the coronae, as well as for isotropic and anisotropic corona deformations, depending on the specific particle morphology and surface pressure. This augmented approach can effectively capture many-body effects without the need for adding many-body potentials.[64−68] As argued below, this simulation methodology not only reproduces the well-established continuous and heterostructural transitions but also naturally captures the 2D isostructural transition in single-component systems.

To accurately reflect the essential features of each particle system in simulations, we recognize that (i) the effective particle size at a given surface pressure follows from the particle softness, (ii) the softness effectively follows from the swollen nature of the polymer network, and (iii) the cross-linking gradient within this network sets the degree of isotropy; that is, whereas loose polymer chains at the interface may behave independently of each other to yield an anisotropic (2D) corona deformation, more cross-linked chains must behave in a more concomitant and therefore more isotropic manner. We account for these effects by letting the typical equilibrium interaction ranges σ_{ij} between particles i and j evolve as augmented, dynamical variables that can vary between extended and collapsed states depending on the local particle environment. We also note that within our approach, and similar to standard coarse-grained simulations of binary mixtures,[69] the size of individual particle i is not an explicit model parameter but rather follows implicitly from the pair interaction parameter σ_{ij}. Importantly, this also allows us to describe anisotropic particle deformations in the case of nonuniformly cross-linked shells, namely, by letting σ_{ij} and $\sigma_{ij'}$ differ among two neighboring particles j and j'. For visual purposes, we will assume that the effective particle radius r_i is given by $r_i = r_{i,\min} = \min_j(\sigma_{ij}/2)$, where index j runs over all possible neighbors of particle i.
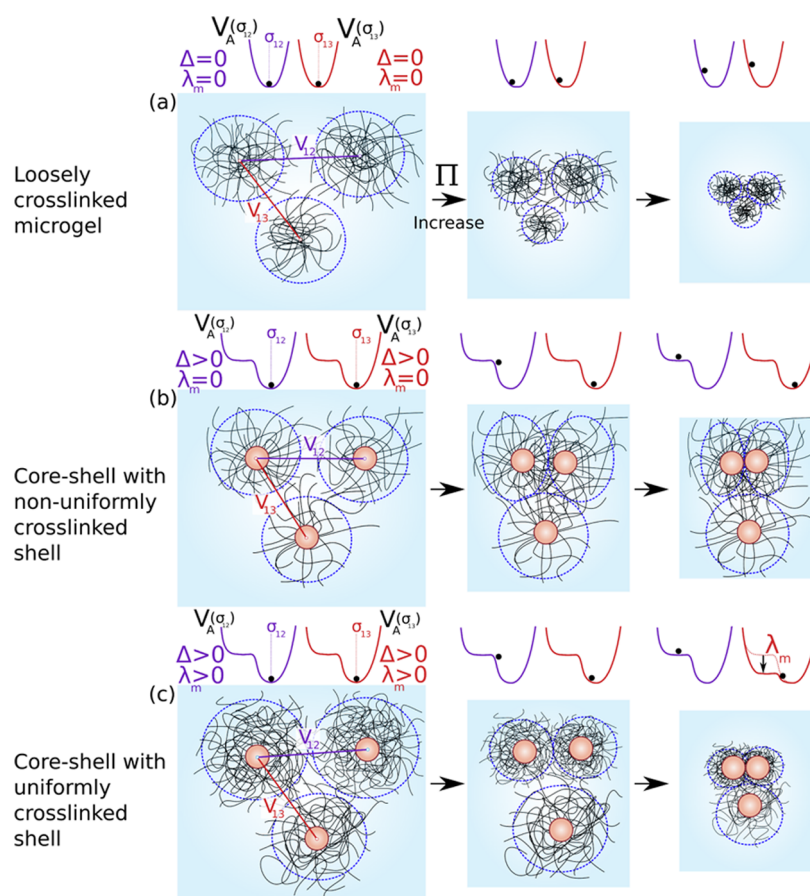
Figure 2. Augmented potential-based simulation scheme used to capture the different interfacial morphologies and simulate the resulting phase behavior. (a–c) Schematic illustration of the response of the different particle systems to compression. The average shape is indicated by dashed blue lines. To model the effect of the compression on the particle shape and to capture all of the phase transition regimes, we use augmented potentials as a function of the interaction distance σ_{ij}, as indicated on top of the individual schematics. (a) Shape of loosely cross-linked microgel particles is represented by setting a barrierless ($\Delta = 0$) augmented potential (eq 2) to mimic the fact that such particles always push to expand to their equilibrium size and by excluding many-body effects ($\lambda_m = 0$). (b) The shape of core–shell particles with a nonuniformly cross-linked shell is represented using $\Delta > 0$ in the augmented potential defined in eq 2, thus creating a metastable state that corresponds to core–core contacts that can be reached for sufficiently high surface pressure. (c) Uniformly cross-linked shells are modeled by including multibody effects. In contrast to loosely cross-linked shells, this particle system is only allowed to collapse isotropically; this effectively reduces the repulsion among all neighboring particles in a strongly correlated manner. We simulate this multibody effect by setting $\lambda_m > 0$. See the Materials and Materials section for more details.

As detailed in the Materials and Methods section and further below, we can capture all three experimental particle systems by tuning only two parameters: an energy barrier Δ that sets the presence of distinct internal length scales in the particle morphology and a parameter λ_m that sets the degree of isotropy in particle compression and therefore the strength of multibody interactions. For all bare pair interactions, we use a generalized Lennard-Jones (LJ) potential. While this choice of potential is a relatively simple approximation for microgel interactions, it is able to phenomenologically capture attractive and low-compression capillary effects, and furthermore, its short-ranged nature allows for computational efficiency. Additionally, the augmented potential approach can be extended to describe multicomponent mixtures.[70] We choose the potential parameters such that the preferred particle sizes in simulations are consistent with the experiment, as explained in more detail in the Materials and Methods section. In Figure 2, we sketch our augmented potential and the corresponding physical scenarios; the augmented potentials are also discussed in more detail in Figure 6a.

Collective Interfacial Phase Behavior. We now analyze the collective phase behavior of the three distinct soft-particle systems confined at a 2D liquid interface. Experimentally, we characterize the systems at the air/water interface using the simultaneous compression and deposition method[17,23] and employ ex situ scanning electron microscopy (SEM) combined with custom-written image analysis software (details in Supporting Information) to establish the different structural phases. The surface pressure–area density curves for the different systems are shown in Figure S1b. As expected, the loosely cross-linked microgels (sample 1; 1 mol % BIS) show the largest interfacial areas. Both core–shell particle types exhibit comparable surface pressure–area density curves that are shifted to lower microgel areas as a result of the solid core and higher cross-linker concentration (sample 2, 3; 5 mol % BIS). One notable difference between the core–shell systems is the shift to lower areas per particle for sample 2, especially at high compression. This shift reflects the larger compressibility of the thinner corona in the particle system with nonuniform cross-linking density, Figure S1c. We compare the observed interfacial phase behavior to the results of our augmented potential model and discuss how the phase behavior can be ultimately rationalized from the molecular architecture via the differences in interfacial morphology.
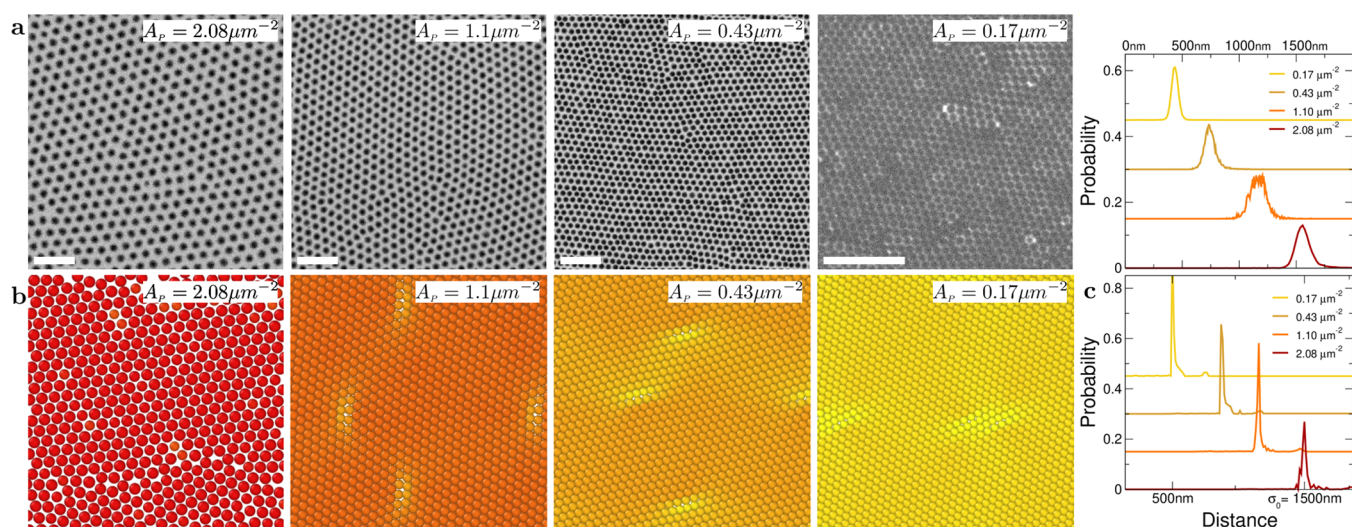
Figure 3. Microgels with a very low cross-linking density behave according to the continuous regime. Comparison between experimentally observed phases (a) and simulations with augmented potentials ($\Delta = \lambda_m = 0$) (b) for microgel particles showing a continuous transition from a hexagonal non-close-packed to a close-packed phase. The area per particle A_P decreases from the left to right. The experimental scale bar is 5 μm, while simulated particles are red in their expanded size and follow a gradient toward yellow during compression. The microgel particles gradually shrink upon compression while preserving their hexagonal lattice. A statistical analysis of the distributions of the nearest-neighbor distances upon compression is shown for both experiments and simulations (c). Data sets are progressively shifted vertically by 0.15 for clarity.
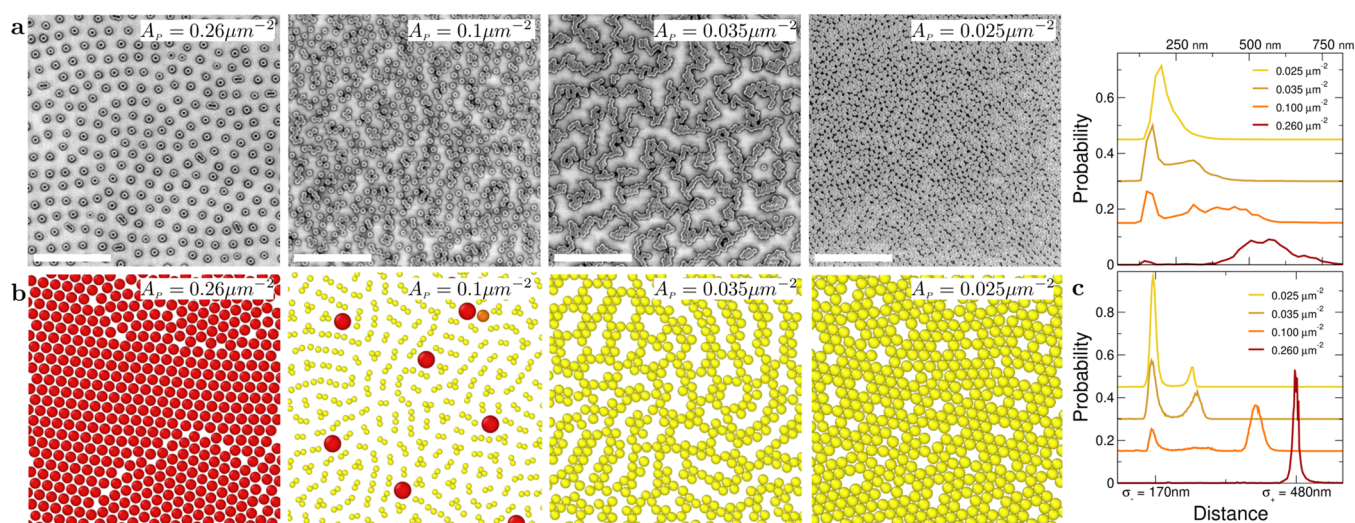

Figure 4. Core−shell particles with nonuniform cross-linked distribution in the shell behave according to the heterostructural regime. Comparison between experimental phases (a) and simulations with augmented potentials ($\Delta > 0$, $\lambda_m = 0$) (b) showing a heterostructural transition from a hexagonal non-close-packed to a chain to a hexagonal close-packed phase. The area per particle A_P decreases from the left to right. The experimental scale bar is 2.5 μm, while simulated particles are red in their expanded size and follow a gradient toward yellow while collapsing. Signatures of the heterostructural transition are the chains of collapsed particles forming at intermediate compression. (c) shows the distribution of the nearest-neighbor distance upon compression. Data sets are progressively shifted vertically by 0.15 for clarity.

Loosely Cross-Linked Particles: Continuous Regime. Upon compressing microgels with a low cross-linking density (particle system (1)), an interfacial behavior classified as the continuous regime is found. The name continuous refers to the fact that the lattice spacing decreases continuously, while no second-order phase transition is observed. Indeed, Figure 3 shows the distinctive uniform shrinkage of microgels upon compression, giving rise to a continuous transition from a non-close-packed to a close-packed hexagonal order. This continuous regime is not generally observed for pure microgels. Indeed, as we discuss below, such systems, especially with higher cross-linking densities, typically exhibit isostructural phase transitions.[23−27]

The continuous regime is exclusively observed for very soft microgels with low cross-linking densities.[24]

In our experiments, the softness is associated with the characteristic stretched-out morphology of such particles visible in the AFM images taken in the dry state (Figure 1(1)). In agreement with results from different simulation approaches, we infer that these particles assume a semispherical morphology at the liquid interface. This quasi-three-dimensional structure causes a rapid increase of overlap volume between the coronae of two neighboring microgel particles upon compression at the interface, i.e., with increasing surface pressure.[71] Assuming that the net (repulsive) interaction energy is proportional to the overlap volume of the coronae and that the overlap volume
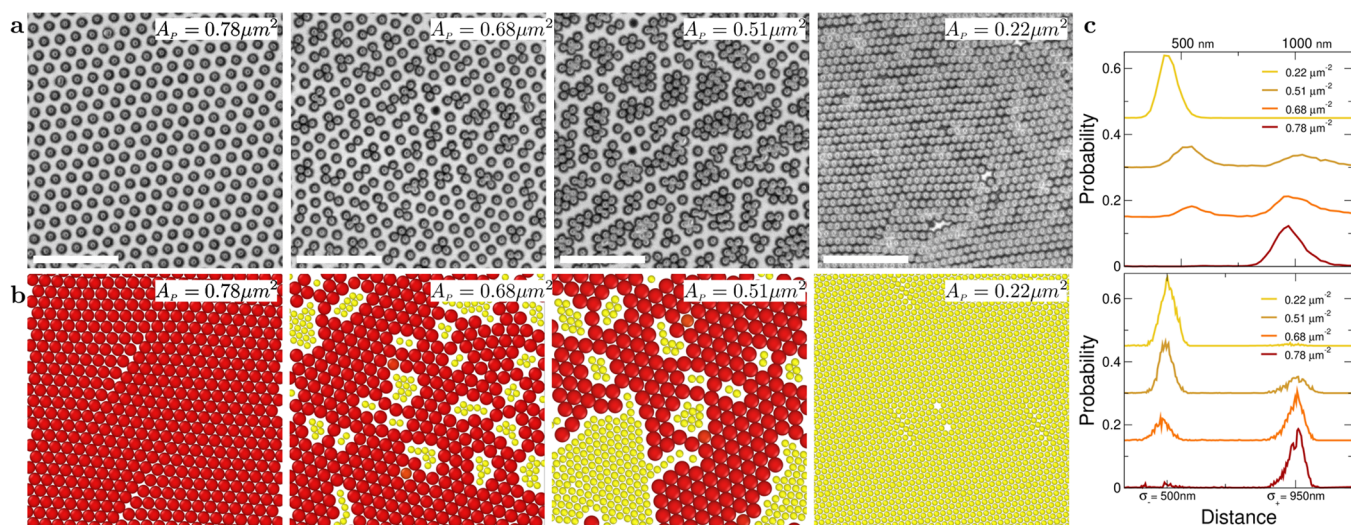
Figure 5. Core−shell particles with a uniformly cross-linked shell behave according to the isostructural regime. Comparison between experimental phases (a) and simulations with augmented potentials ($\Delta > 0$, $\lambda_{\mathrm{m}} > 0$). (b) Transition from hexagonal non-close-packed to hexagonal close-packed. The area per particle A_{P} decreases from the left to right. The experimental scale bar is 5 μm, while simulated particles are red in their expanded size and follow a gradient toward yellow while collapsing. A characteristic of the isostructural transition is the coexistence of clusters of collapsed particles and expanded particles at intermediate surface pressure. (c) Distribution of the nearest-neighbor distance upon compression. Data sets are progressively shifted vertically by 0.15 for clarity.

between quasi-three-dimensional spheres grows nonlinearly with the particle−particle distance, it follows that the repulsion rapidly increases with compression. This effectively forces the particles to simply pack closer together in a continuous manner.

The continuous regime also naturally appears in our augmented simulation approach with a single equilibrium distance corresponding to two expanded microgels in contact (Figure 2a). We recall that the continuous regime can also be captured by simpler[36,44] or more refined[72] coarse-grained models using convex repulsion potentials. In the augmented scheme, this convexity appears in both the particle−particle interaction and the augmented potential; in fact, the augmented potential V_{A}, which we use to describe this microgel system, is always convex if we set $\Delta = 0$ (see the Materials and Methods section). As shown in Figure 3, our simulations closely reproduce the experimental phase behavior: a decrease in the area per particle preserves the hexagonal lattice but monotonically decreases the lattice constant.

The statistical distribution of nearest-neighbor distances further underscores that the continuous transition is adequately captured both in experiments and simulation (Figure 3c). It can be seen that the typical interparticle distance and thus the lattice spacing decrease continuously upon compression. This behavior is consistent with the fact that such particles lack a defined core and therefore do not possess an additional internal length scale, rendering our augmented potential with a single length scale ($\Delta = 0$) suitable for modeling.

Core−Shell Particles with a Nonuniformly Cross-Linked Shell: Heterostructural Regime. Figure 4 shows the experimental and numerical results for the heterostructural transition regime, which exhibits phase transitions from a hexagonal non-close-packed phase to a characteristic, network-forming chain phase and finally to a hexagonal close-packed structure upon compression. The transition is further confirmed in the nearest-neighbor distance distribution, which reveals the chain phase by the coexistence of collapsed and more extended particle pairs. The two peaks that appear as satellites at the highest compression in simulations are related to diagonal nearest

neighbors, found for particles in double chains or more compressed states with multiple neighboring particles in contact. In the experiments, these peaks are not accurately resolved at the highest compression, but the anisotropic shape of the nearest-neighbor peak hints at similar pairs. Our experimental data with nonuniformly cross-linked particles (particle system (2)) constitute the first single-component system exhibiting such a heterostructural transition. Previously, the only observed chain phases occurred in soft binary mixtures with similar assumed interfacial morphologies.[71,73,74]

The ability to achieve this phase transition experimentally stems from the theoretical insights gained from our simulations (Figure 2), which demand not only two distinct internal particle length scales but also an anisotropic type of interaction, such that σ_{ij} and $\sigma_{ij'}$ can be distinct for a given particle i with neighbors j and j'. We can realize both of these requirements in core−shell particles with a nonuniform cross-linked distribution in the shell and, thus, more loosely connected polymer chains in the periphery. To understand the rationale behind this, let us first recall from Figure 1(2) that these particles assume a pronounced core−corona morphology with a well-defined hard-core and a thin, quasi-two-dimensional corona when adsorbed at the liquid interface. The clear distinction between the core and corona naturally satisfies the two-length-scale prerequisite. The second condition requires the corona to be anisotropically compressible at the interface in any direction. Physically, this enables the system to leverage a tradeoff in repulsive corona overlaps upon compression: rather than letting all pairs of particles undergo a partial, uniform overlap (or collapse) of their coronae, the system may minimize its total free energy by avoiding any overlap among neighboring particles in one direction, at the cost of fully overlapping in another. This leads to a chain phase in which the intrachain interactions correspond to core−core contacts, while the interactions between adjacent chains are governed by extended corona−corona contacts. On the molecular level, such anisotropic corona deformations can be achieved by loosely connected polymer chains that can interact with neighboring particles independently from one another.

Thus, the ideal corona should consist of many individual long polymer chains with as few chemical or physical cross-linking points as possible. The experimental results in Figure 4 suggest that our chosen particle morphology realizes this scenario, indicating that in the batch synthesis method the cross-linker is indeed mainly integrated around the inner region of the polymer shell. Finally, with these findings, we can also infer why previous experimental studies on core−shell particles have not found heterostructural transitions, namely, due to a too high cross-linking density in the periphery that prevents anisotropic corona interactions.

In contrast to experiments, the heterostructural regime is less difficult to find in silico and has been theoretically predicted decades ago for particles interacting via soft repulsive, Jagla-type potentials.[36,44,45] Indeed, since many-body correlation effects can be ignored due to the flexibility of the coronae in all directions, it suffices to let particles interact through a relatively simple pairwise potential. This interaction, however, must include two different length scales to account for the distinct core−core and corona−corona contacts. For Jagla-like potentials used in standard MD simulations, one has to be careful and additionally destabilize the continuous regime by invoking a nonconvex potential (or $g > 1$ in Jagla's terminology).[71] We note that this Jagla-based perspective can also be united with the observed interfacial morphology (Figure 1(2)). Again assuming that the repulsive interaction energy scales with the overlap volume, we expect a near-linear ramp potential for two-dimensional corona morphologies, as opposed to the more semispherical conformations discussed in the previous section.[71] In our simulation scheme, we rely on the augmented potential V_A by setting $\Delta > 0$ to incorporate the two required length scales, without a stringent convexity requirement on the bare interaction potential (Figure 2b). An additional advantage of this augmented ensemble approach over the Jagla approach is that particles can also be attractive (see the Materials and Methods section and eq 1) to account for, e.g., low-compression capillary effects.[75]

Core−Shell Particles with a Uniformly Cross-Linked Shell: Isostructural Regime. The third phase regime concerns the isostructural phase transition of soft particles. In Figure 5, we show the results obtained from our augmented simulations, combined with the corresponding experimental results for core−shell particles with a uniformly cross-linked distribution in the shell. The distinctive growth of close-packed hexagonal clusters is evident at intermediate compression for both simulations and experiments. Furthermore, the histograms in Figure 5c show a bimodal distribution of interparticle distances, corresponding to either expanded or collapsed pairs. A small shift of the compressed peak can be seen in the experimental data, which is not resolved in the simulations. In the simulations, the particles can only form large or small contacts, given by the two energy minima. In the experiments, although the solid core provides a physical barrier toward further collapse, there is still microgel in between the cores even in the collapsed region. This microgel layer can apparently be slightly compressed in the course of the experiment.

To understand the physical origins of the discontinuous isostructural transition, we first recognize that particles must exhibit a sharp and isotropic collapse upon compression. Naturally, the sharp distinction between a collapsed and extended state also requires two internal particle length scales. Core−shell particles with a relatively densely and uniformly cross-linked shell (particle system (3)) are a typical example of

such particles. Figure 1(3) shows their interfacial morphology, clearly satisfying the prerequisite of having two distinct length scales. Additionally, with the continuous-feeding synthesis method, the resulting polymer shells contain more uniformly distributed cross-linking points, which is consistent with the continuous decrease in height from the core to the periphery, as seen in Figure 1(3). In this molecular architecture, the chains are much more constrained by the presence of crosslinkers across the entire volume of the shell, which reduces both the length of free dangling chains at the periphery and the freedom of the chains to move independently from each other. Upon compression, such uniformly cross-linked particles are therefore forced to distribute the stress across the entire shell. This, in turn, prohibits the formation of a chainlike phase since the corona is no longer able to collapse in one direction while simultaneously remaining extended in another. Instead, we postulate that the collapse of any pair of particles now imposes a shrinkage of the coronae in all directions and thus facilitates collapse events with other neighboring particles, favoring an isostructural transition. The collapse event is also affected by the particle core. For larger core sizes, capillary attraction increasingly destabilizes the interfacial corona−corona morphology and therefore facilitates the isostructural transition.[12,21] Noteworthily, the isostructural phase transition is also often observed in conventional microgel systems without a solid core.[23−27,31] In this case, we hypothesize that the required two length scales arise from the typical fried-egg or core−corona morphology that microgels assume at the interface. This morphology, caused by a higher cross-linking density within the core region, leads to a stiffer and therefore less compressible core.[19,20,22]

From the modeling side, the isostructural regime has been difficult to capture in standard MD simulations. For example, the Jagla potential only predicts a continuous transition between the two hexagonal phases and not an isostructural phase transition, regardless of the chosen pair potential.[45,71,74] From our insights, we can attribute these earlier discrepancies to the fact that pairwise potentials in conventional MD models impose interactions that are fixed a priori so that all particle pairs always interact in the same way at a given interparticle distance. However, in reality, an isotropic particle collapse induced by one neighbor will concomitantly affect the interactions with all other neighboring particles. Indeed, it follows from the interconnected polymer shell that the collapse will lead to a significant change in particle conformation in all possible directions. To adequately model the isostructural regime, it is therefore crucial to incorporate local many-body effects into the simulations such that any isotropic particle deformation is immediately translated to a change in the net pair potentials with neighboring particles.

Keeping these considerations in mind, we can adopt our augmented simulation scheme to describe the isostructural regime. Specifically, we account for distinct collapsed and extended states by setting $\Delta > 0$ in the augmented potential V_A; for the required local many-body effects, we impose one additional constraint by setting $\lambda_m > 0$ (Figure 2c). To understand the latter, let us first recall that in the heterostructural regime every particle i is allowed to interact independently (i.e., with a different σ_{ij}) with each of its neighbors j. A pair ij can then either be in an expanded state $\sigma_{ij} \sim \sigma_+$ or, if compressed, in a collapsed state $\sigma_{ij} \sim \sigma_-$. In the isostructural regime, we assume that once a particle i collapses with one of its neighbors such that the minimum particle radius becomes $r_{i,\min} < \lambda_m \sigma_-/2$, it will also immediately collapse with all

of the other neighbors j that are already involved in a collapse elsewhere (i.e., with $r_{j,\min} < \lambda_m \sigma_-/2$). Subsequently, we then impose that $\sigma_{ij} = r_{i,\min} + r_{j,\min} = \sigma_-$. This mimics the effect that each collapse after the first is facilitated by the presence of other collapsed particles nearby, as we sketch in the bottom right panel of Figure 2. When $\lambda_m = 0$, this effect is suppressed and each pair collapses individually. When $\lambda_m \sim 1$, this multibody interaction becomes relevant because the resulting $\lambda_m \sigma_-/2$ is an available state. Note that this also effectively suppresses the formation of chainlike structures since a stable chain phase would require that $\sigma_{ij} = \sigma_+$ for interactions between particles in adjacent chains (also see the Materials and Methods section and Figure 7).

CONCLUSIONS

In this work, we put forward a multiscale-based perspective of soft-particle behavior at liquid interfaces, allowing us to relate collective interfacial phase behavior to the interfacial morphology and the molecular architecture of soft particles. We study three archetypal soft particles that exhibit the characteristic phase behaviors of continuous, heterostructural, and isostructural transitions. Our experimental observations are supported by an augmented variable simulation model that is able to capture all experimentally observed phase transitions—including the elusive 2D isostructural transition—by tuning only two coarse-grained model parameters.

The general insights inferred from this work can be summarized as follows:

(i) The continuous transition is characterized by a single length scale and repulsion energy that increases nonlinearly (convexly) with the particle−particle distance. Soft particles without a hard-core and a loosely cross-linked structure are the perfect prototypes for this continuous regime since their quasi-semi-spherical interfacial morphology can be assumed to yield a net convex interaction potential.

(ii) For a heterostructural phase transition, where non-close-packed and close-packed hexagonal phases are separated by other ordered phases such as chains, a core−shell particle with two distinct internal length scales is required. Additionally, the corona needs to be anisotropically compressible to allow particles to collapse in one direction, i.e., within a chain, while avoiding overlap in another, i.e., between two adjacent chains. We demonstrate that this phase behavior can be experimentally realized for core−shell particles with a nonuniformly cross-linked shell, where the periphery consists of long dangling chains with minimal cross-linking.

(iii) At last, the isostructural regime, which is characterized by a discontinuous transition from a non-close-packed to close-packed hexagonal phase, also requires two internal particle length scales, either provided by a core−shell architecture or via the inhomogeneous cross-linking densities of pure microgels. However, as opposed to the heterostructural case, the particles must collapse isotropically to distribute the pressure load in every direction. Experimentally, this behavior is favored by a more uniformly cross-linked shell that forces the polymer chains to compress in a concomitant manner. Theoretically, the effect of such isotropic shell deformations gives rise to local many-body correlations with neighboring particles, which in turn facilitates nearby particle collapses

to ultimately yield a complete and discontinuous isostructural phase transition.

It is our hope that this framework, which qualitatively links the molecular architecture of soft particles to their interfacial particle morphology and resulting collective phase behavior, can serve as a starting point for an ultimately more quantitative and predictive rational-design platform. To this end, efforts in the quantitative characterization of the interfacial morphology, for example, by scattering methods, are required, which may allow determination of critical parameters marking the transition between the different regimes. Such efforts will not only provide a better fundamental understanding of soft materials at the interface but can also stimulate the discovery of new self-assembled structures by rationally targeting molecular architectures required for more complex, theoretically predicted assembly phases.

MATERIALS AND METHODS

Experiments. A detailed description of the PNIPAM-based core−shell particle synthesis by precipitation polymerization can be found in previous work[12,24] and in the Supporting Information. In short, PNIPAM microgel particles (continuous regime) with 1 mol % cross-linker (N,N'-methylenebisacrylamide) (BIS) were synthesized in a one-pot reaction.[24] Silica−PNIPAM core−shell particles undergoing a heterostructural phase transition were obtained by surface functionalization of Stöber silica cores (d_C = 160 nm) with methacrylate moities to anchor the polymer shell to the surface. Then, a PNIPAM microgel shell (5 mol % BIS) was added onto the cores in a one-pot, batch method. For the core−shell particles undergoing an isostructural phase transition, we used the same synthesis as above but continued to add additional monomer and cross-linker via a continuous-feeding process (5 mol % BIS).[12] The interfacial phase diagram of the core−shell particles at the air/water interface was obtained by the simultaneous compression and deposition method[23,24] using a Langmuir trough followed by characterization using SEM (Zeiss Gemini 500). The morphology was investigated by AFM (JPK NanoWizzard) in the AC mode using a MikroMash NSC-18/AL BS cantilever.

Simulation Model: Augmented Ensemble. In our simulations, two particles separated by a distance r_{ij} interact through the following potential[63]

$$V(r_{ij}, \sigma_{ij}) = \begin{cases} 6\epsilon\left[\left(\dfrac{\sigma_{ij}}{r_{ij}}\right)^{12} - \left(\dfrac{\sigma_{ij}}{r_{ij}}\right)^{6} + \displaystyle\sum_{l=0}^{3} c_{2l}\left(\dfrac{r_{ij}}{\sigma_{ij}}\right)^{2l}\right], & \dfrac{r_{ij}}{\sigma_{ij}} < x_c \\ 0, & \dfrac{r_{ij}}{\sigma_{ij}} \geq x_c \end{cases}$$

(1)

which is a modified Lennard-Jones (LJ) potential with energy well depth ϵ. Parameter σ_{ij} is the sum of the radius σ_i of particle i and the radius σ_j of particle j. The potential is plotted in Figure 6b for different values of σ_{ij}. The coefficients c_{2l} are determined by requiring that the first three derivatives of V vanish at the adimensional cutoff distance x_c = 2. These corrections to LJ are fundamental in the augmented ensemble because the cutoff distance might be coupled to augmented variables and can thus change over time, preventing the use of constant tail corrections.[76] It is important to use an attractive potential to model the capillarity effect at the interface.[75]

Augmented Potentials. Augmented potentials and variables are phenomenologically built to closely reproduce experimental results, similarly to fictitious pairwise potentials.[77,78] In this section, we explain the physics behind them. The first step is the choice of what augmented variables represent. In the Supporting Information, we use σ_i as augmented variables, following refs 63 and 79. We show that this approach is well suited to model particles that can expand and collapse, which is the case for, e.g., polymer stars, coils, brushes,[80,81] and
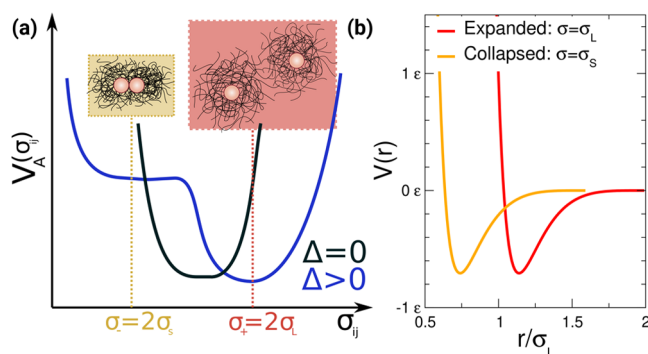
Figure 6. (a) Augmented potentials as a function of the interaction distance σ_{ij}. The black line represents eq 2 when $\Delta = 0$, such that the potential is effectively $(\sigma_{ij} - \sigma_0)^8$. The blue line corresponds to $\Delta > 0$, provoking the appearance of a second length scale. The minimum at $\sigma_+ = 2\sigma_L$ represents the favorable situation of expanded particles, while the metastable minimum at $\sigma_- = 2\sigma_S$ is the collapsed state. (b) Pairwise potential defined in eq 1 as a function of the central distance r. Since the interaction distance is treated as a variable, the potential can shift over time. See the Materials and Methods section for more details.

responsive particles.[19,82−84] However, the soft particles that we want to model here can collapse only when the reciprocal pressure of a pair of particles exceeds the threshold, so it is not possible to have a single collapsed particle between only expanded neighbors. We model this feature by using the interaction distances σ_{ij} as our augmented variables. If σ_{ij} is large, then we have a pair of widely spaced expanded particles, while if σ_{ij} decreases the two particles can get closer as if they are collapsing. Noticeably, the dynamics of σ_{ij} is coupled to the positions by the pairwise potential since eq 1 does depend on σ_{ij}. This produces a force acting on σ_{ij} equal to $-\partial V(r_{ij}, \sigma_{ij})/\partial\sigma_{ij}$. To bound the augmented variables in a physical regime, we add an external augmented potential $V_A(\sigma_{ij})$ that acts only on the augmented variables. The potential has to be phenomenologically built to reproduce the correct physics of the system. In particular, we propose

$$V_A(\sigma_{ij}) = K[(\sigma_{ij} - \sigma_0)^4 - \Delta]^2 - 5K\Delta(\sigma_{ij} - \sigma_0) \quad (2)$$

which is based on a standard double-well potential with a barrier height of $K\Delta^2$ (represented by the first term of eq 2). The values of σ_0 and Δ control the position of two (or one for $\Delta = 0$) minima $\sigma_\pm = \sigma_0 \pm \Delta^{1/4}$. Setting $\Delta = 0$ is an easy way to model (in the augmented ensemble) particles whose stiffness increases with compression, the fundamental requirement of the continuous regime. Alternatively, $\Delta > 0$ introduces the two length scales required for the heterostructural and isostructural regimes. For the simulations reported in Figures 3, 4, and 5, we calculate the precise values of σ_0 and Δ that match the experimental measurements (measured and reported in the Supporting Information): $\sigma_0 = 1500$ nm is the preferred size in the continuous regime, $\sigma_+ = 480$ nm and $\sigma_- = 170$ nm are the two length scales in the heterostructural regime, and $\sigma_+ = 950$ nm and $\sigma_- = 500$ nm for the isostructural case. Consequently, we are able to see the effect of the compression at the same area per particle that we measure in the experiments. Furthermore, we add to the double-well potential a linear term to favor the configurations with $\sigma_{ij} \sim \sigma_+$ to model the fact that a pair of microgels prefers to stay at its expanded size, where the polymer chains have more space to move. The particular coefficient $-5K\Delta$ we use in eq 2 is calculated imposing that $V_A(\sigma_-) - V_A(\sigma_+) = 10K\Delta^2$ corresponding to 10 times the energy barrier such that the configurations with $\sigma_{ij} \sim \sigma_-$ are very short-lived and thus only favorable at high compression. At last, the prefactor K represents the overall magnitude of the potential that dictates the energy scale and thus the stiffness of the particle. Then, the augmented variables evolve following the augmented force F_A

$$-F_A(\sigma_{ij}) = \frac{\partial V(r_{ij}, \sigma_{ij})}{\partial\sigma_{ij}} + \frac{\partial V_A(\sigma_{ij})}{\partial\sigma_{ij}} \quad (3)$$

leading to the equation of motion

$$m_\sigma \ddot{\sigma}_{ij}(t) = F_A(\sigma_{ij}) \quad (4)$$

where m_σ is a fictitious mass for the σ_{ij} dynamics. In the Suppporting Information, we write down the full (pseudo)-Hamiltonian that governs the equations of motion.

We plot the augmented potentials in Figure 6a. It is clear that the energetically favored states correspond to $\sigma_{ij} \sim \sigma_+$. That value represents two particles in contact while being at their maximum size in the expanded state of radius σ_L, so $\sigma_+ = 2\sigma_L$. To collapse to the small size of $\sigma_- = 2\sigma_S$, the pair has to spend some energy and cross the barrier. Numerically, σ_+ and σ_- correspond to the average diameter of particles in the collapsed and expanded AFM pictures, respectively. Furthermore, the V_A collapsed state is made metastable by the linear term such that particles always expand if not compressed. Since σ_{ij} can change, it means that the pairwise interaction in eq 1 has to readjust according to the global and local environment probed by σ_{ij}. In this sense, we show in Figure 6b that the equilibrium length becomes smaller for collapsed pairs.

At last, with the support of Figure 7, we discuss the effect of many-body interactions to distinguish between the heterostructural and isostructural simulations. Since every particle i is involved in N
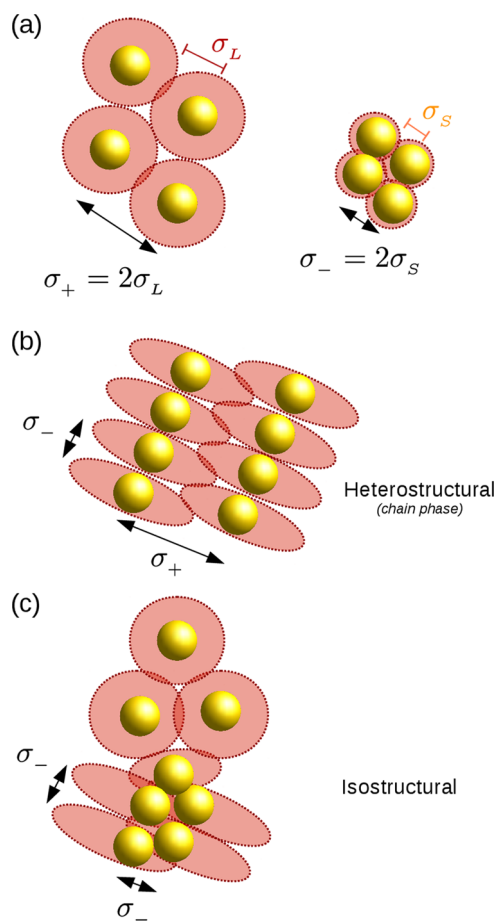

Figure 7. Effect of the augmented potential on the particle size. (a) Stable state $\sigma_{ij} = \sigma_+$ corresponds to two expanded particles of size σ_L in contact, while the metastable $\sigma_{ij} = \sigma_-$ corresponds to the contact of two collapsed particles of size σ_S. (b) In the heterostructural regime, chainlike structures are stable for intrachain interaction ranges of $\sigma_{ij} = \sigma_-$ and interchain interaction ranges of $\sigma_{ij} = \sigma_+$. (c) In the isostructural regime, setting $\lambda_m > 0$, we impose that if a particle is collapsed in the chain direction it is also more likely to collapse with its other neighbors, creating the typical close-packing hexagonal domains.

interactions with all of the others j, the simplest way to define the size of each particle is through

$$r_{i,\mathrm{min}} = \min_{j} \frac{\sigma_{ij}}{2} \qquad (5)$$

We say that a particle is collapsed if $r_{i,\mathrm{min}} \sim \sigma_S$, so i has to reduce the value of σ_{ij} with just one of its neighbors j to be considered collapsed. As a consequence, even if $r_{i,\mathrm{min}} \sim r_{j,\mathrm{min}} \sim \sigma_S$, it is possible that $\sigma_{ij} \gg \sigma_- = 2\sigma_S$. This means that two particles that are collapsed might still have a long range repulsion that requires additional energy to eventually collapse. From a microscopic point of view, this extra repulsion is attributed to the loosely cross-linked shell, which, being characterized by long dangling polymer chains, is able to rearrange to occupy more space around the core−core contacts. This effect (sketched in Figure 7b) leads to chain formation because particles want to assume a phase where the contacts are minimal, so all of the energy is invested in collapsing only two contacts per particle within the chains, producing the heterostructural regime. Finally, to describe the isostructural regime, we have to prevent this anisotropic effect. We do so by imposing that if $r_{i,\mathrm{min}} + r_{j,\mathrm{min}} < \lambda_{\mathrm{m}}\sigma_- \rightarrow \sigma_{ij} = \sigma_-$. We set $\lambda_{\mathrm{m}} = 0$ (no multibody effects) to reproduce the results in Figures 3 and 4, while we set $\lambda_{\mathrm{m}} = 1.01$ to produce Figure 5. This additional λ_{m}-dependent rule mimics the effect of isotropic compression such that a partial collapse induced by one neighboring particle will be felt by all neighbors; these in turn can then stimulate a full collapse. This also suppresses the chain phase that requires $\sigma_{ij} = \sigma_+$ to stabilize the interactions between neighboring chains, as we show in Figure 7c.

Computational Details. We perform two-dimensional MD simulations with periodic boundary conditions to model the interfacial layer. All of our interfaces are equilibrated in the canonical NVT ensemble, at constant particle number $N = 500$ and temperature T; the volume $V = L^2$ is used as the control parameter. We use the leap-frog integration method coupled to a Berendsen thermostat[85] to keep T constant, and we vary L to approach the desired area per particle $A_P = L^2/N$. After equilibrating the interface for 10^6 time steps of size d$t = 10^{-3}$ reduced units at $T = 2\epsilon$ and large A_P, we gradually compress the system reducing L and in turn A_P. During the compression, we use the FIRE algorithm[86] to minimize the energy and find the inherent structure at target A_P, mimicking the experimental quench that happens at the interface. As discussed in the previous section, the values of Δ and σ_0 are dictated by the experiments: (i) $\sigma_0 = 1500$ nm is the preferred size in the continuous regime (and $\Delta = 0$ to have a single minimum), (ii) $\sigma_+ = 480$ nm and $\sigma_- = 170$ nm set σ_0 and Δ for the heterostructural regime, and finally (iii) $\sigma_+ = 950$ nm and $\sigma_- = 500$ nm determine σ_0 and Δ in the isostructural regime. The stiffness parameter instead dictates the response of the microgels to compression, and we tailor it to reproduce the experimental measurements by using the following values: $K = 0.01$ ϵ nm^{-8} for the continuous regime (Figure 3), $K = 1$ ϵ nm^{-8} for the heterostructural regime (Figure 4) and $K = 0.05$ ϵ nm^{-8} for the isostructural regime (Figure 5), where ϵ is the unit of energy. For the many-body interactions, we set $\lambda_{\mathrm{m}} = 0$ to disable such effects in the continuous and heterostructural regimes, while we set $\lambda_{\mathrm{m}} = 1.01$ to obtain the isostructural regime. The last unit that we set is the augmented mass $m_\sigma = m = 1[M]$ that represents the inertia of the augmented variable, dictating how rapidly a pair can change σ_{ij}, and we sat that equal to the ordinary mass m. The importance of the augmented potential compared to the standard LJ interaction can be tweaked either through K or m_σ, but we suggest to modify K and let $m_\sigma = m$ to avoid numerical instabilities. We repeat the procedure for $M > 50$ randomly generated configurations to verify the consistency of the results and get better statistics for the histograms.

ASSOCIATED CONTENT

ⓈⒾ Supporting Information

The Supporting Information is available free of charge at https://pubs.acs.org/doi/10.1021/acs.langmuir.1c00541.

Additional information about the augmented ensemble simulation with a general example of particle size as an augmented variable, experimental details of the materials and synthesis used, and characterization of the experimental systems through dynamic light scattering (PDF)

Visualization of the simulation protocol for the different particle architectures, represented by different augmented potentials (MP4)

AUTHOR INFORMATION

Corresponding Authors

Nicolas Vogel − *Institute of Particle Technology, Friedrich-Alexander University Erlangen-Nürnberg, 91058 Erlangen, Germany;* ◉ orcid.org/0000-0002-9831-6905; Email: nicolas.vogel@fau.de

Liesbeth M. C. Janssen − *Department of Applied Physics, Eindhoven University of Technology, 5600 MB Eindhoven, The Netherlands;* Email: l.m.c.janssen@tue.nl

Authors

Simone Ciarella − *Department of Applied Physics, Eindhoven University of Technology, 5600 MB Eindhoven, The Netherlands*

Marcel Rey − *Institute of Particle Technology, Friedrich-Alexander University Erlangen-Nürnberg, 91058 Erlangen, Germany;* ◉ orcid.org/0000-0002-1721-0253

Johannes Harrer − *Institute of Particle Technology, Friedrich-Alexander University Erlangen-Nürnberg, 91058 Erlangen, Germany*

Nicolas Holstein − *Institute of Particle Technology, Friedrich-Alexander University Erlangen-Nürnberg, 91058 Erlangen, Germany*

Maret Ickler − *Institute of Particle Technology, Friedrich-Alexander University Erlangen-Nürnberg, 91058 Erlangen, Germany*

Hartmut Löwen − *Institute for Theoretical Physics II: Soft Matter, Heinrich-Heine University Düsseldorf, D-40225 Düsseldorf, Germany*

Complete contact information is available at:
https://pubs.acs.org/10.1021/acs.langmuir.1c00541

Notes

The authors declare no competing financial interest.

REFERENCES

(1) McGorty, R.; Fung, J.; Kaz, D.; Manoharan, V. N. Colloidal self-assembly at an interface. *Mater. Today* **2010**, *13*, 34−42.

(2) Binks, B. P. Particles as surfactants−similarities and differences. *Curr. Opin. Colloid Interface Sci.* **2002**, *7*, 21−41.

(3) Pieranski, P. Two-dimensional interfacial colloidal crystals. *Phys. Rev. Lett.* **1980**, *45*, 569−572.

(4) Liu, T.; Seiffert, S.; Thiele, J.; Abate, A. R.; Weitz, D. A.; Richtering, W. Non-coalescence of oppositely charged droplets in pH-sensitive emulsions. *Proc. Natl. Acad. Sci. U.S.A.* **2012**, *109*, 384−389.

(5) Destribats, M.; Lapeyre, V.; Sellier, E.; Leal-Calderon, F.; Ravaine, V.; Schmitt, V. Origin and control of adhesion between emulsion drops

stabilized by thermally sensitive soft colloidal particles. *Langmuir* **2012**, *28*, 3744−3755.

(6) Aussillous, P.; Quéré, D. Liquid Marbles. *Nature* **2001**, *411*, 924.

(7) Binks, B. P.; Murakami, R. Phase inversion of particle-stabilized materials from foams to dry water. *Nat. Mater.* **2006**, *5*, 865−869.

(8) Binks, B. P.; Horozov, T. S. Aqueous foams stabilized solely by silica nanoparticles. *Angew. Chem., Int. Ed.* **2005**, *44*, 3722−3725.

(9) Gonzenbach, U. T.; Studart, A. R.; Tervoort, E.; Gauckler, L. J. Ultrastable particle-stabilized foams. *Angew. Chem., Int. Ed.* **2006**, *45*, 3526−3530.

(10) Grillo, F.; Fernandez-Rodriguez, M. A.; Antonopoulou, M.-N.; Gerber, D.; Isa, L. Self-templating assembly of soft microparticles into complex tessellations. *Nature* **2020**, *582*, 219−224.

(11) Fernández-Rodríguez, M. Á.; Elnathan, R.; Ditcovski, R.; Grillo, F.; Conley, G. M.; Timpu, F.; Rauh, A.; Geisel, K.; Ellenbogen, T.; Grange, R.; Scheffold, F.; Karg, M.; Richtering, W.; Voelcker, N. H.; Isa, L. Tunable 2D binary colloidal alloys for soft nanotemplating. *Nanoscale* **2018**, *10*, 22189−22195.

(12) Tang, J. S. J.; Bader, R. S.; Goerlitzer, E. S. A.; Wendisch, J. F.; Bourret, G. R.; Rey, M.; Vogel, N. Surface Patterning with SiO2@PNiPAm Core−Shell Particles. *ACS Omega* **2018**, *3*, 12089−12098.

(13) Goerlitzer, E. S. A.; Mohammadi, R.; Nechayev, S.; Volk, K.; Rey, M.; Banzer, P.; Karg, M.; Vogel, N. Chiral Surface Lattice Resonances. *Adv. Mater.* **2020**, *32*, No. 2001330.

(14) Kaz, D. M.; McGorty, R.; Mani, M.; Brenner, M. P.; Manoharan, V. N. Physical ageing of the contact line on colloidal particles at liquid interfaces. *Nat. Mater.* **2012**, *11*, 138−142.

(15) Vogel, N.; Retsch, M.; Fustin, C.-A.; del Campo, A.; Jonas, U. Advances in Colloidal Assembly: The Design of Structure and Hierarchy in Two and Three Dimensions. *Chem. Rev.* **2015**, *115*, 6265−6311.

(16) Aveyard, R.; Clint, J. H.; Nees, D.; Paunov, V. N. Compression and structure of monolayers of charged latex particles at Air / Water and Octane / Water interfaces. *Langmuir* **2000**, *16*, 1969−1979.

(17) Rey, M.; Fernandez-Rodriguez, M. A.; Karg, M.; Isa, L.; Vogel, N. Poly-N-isopropylacrylamide Nanogels and Microgels at Fluid Interfaces. *Acc. Chem. Res.* **2020**, *53*, 414−424.

(18) Style, R. W.; Isa, L.; Dufresne, E. R. Adsorption of Soft Particles at Fluid Interfaces. *Soft Matter* **2015**, *11*, 7412−7419.

(19) Geisel, K.; Isa, L.; Richtering, W. Unraveling the 3D localization and deformation of responsive microgels at oil/water interfaces: A step forward in understanding soft emulsion stabilizers. *Langmuir* **2012**, *28*, 15770−15776.

(20) Zielińska, K.; Sun, H.; Campbell, R. A.; Zarbakhsh, A.; Resmini, M. Smart nanogels at the air/water interface: structural studies by neutron reflectivity. *Nanoscale* **2016**, *8*, 4951−4960.

(21) Rauh, A.; Rey, M.; Barbera, L.; Zanini, M.; Karg, M.; Isa, L. Compression of hard core−soft shell nanoparticles at liquid−liquid interfaces: influence of the shell thickness. *Soft Matter* **2017**, *13*, 158−169.

(22) Camerin, F.; Fernández-Rodríguez, M. Á.; Rovigatti, L.; Antonopoulou, M.-N.; Gnan, N.; Ninarello, A.; Isa, L.; Zaccarelli, E. Microgels Adsorbed at Liquid−Liquid Interfaces: A Joint Numerical and Experimental Study. *ACS Nano* **2019**, *13*, 4548−4559.

(23) Rey, M.; Fernández-Rodríguez, M. Á.; Steinacher, M.; Scheidegger, L.; Geisel, K.; Richtering, W.; Squires, T. M.; Isa, L. Isostructural solid-solid phase transition in monolayers of soft core-shell particles at fluid interfaces: Structure and mechanics. *Soft Matter* **2016**, *12*, 3545−3557.

(24) Rey, M.; Hou, X.; Tang, J. S. J.; Vogel, N. Interfacial arrangement and phase transitions of PNiPAm microgels with different crosslinking densities. *Soft Matter* **2017**, *13*, 8717−8727.

(25) Picard, C.; Garrigue, P.; Tatry, M.-C.; Lapeyre, V.; Ravaine, S.; Schmitt, V.; Ravaine, V. Organization of microgels at the air-water interface under compression: role of electrostatics and cross-linking density. *Langmuir* **2017**, *33*, 7968−7981.

(26) Scheidegger, L.; Fernández-Rodríguez, M. Á.; Geisel, K.; Zanini, M.; Elnathan, R.; Richtering, W.; Isa, L. Compression and deposition of microgel monolayers from fluid interfaces: particle size effects on

interface microstructure and nanolithography. *Phys. Chem. Chem. Phys.* **2017**, *19*, 8671−8680.

(27) El-Tawargy, A. S.; Stock, D.; Gallei, M.; Ramadan, W. A.; Shams El-Din, M. A.; Reiter, G.; Reiter, R. Multiple Structural Transitions in Langmuir Monolayers of Charged Soft-Shell Nanoparticles. *Langmuir* **2018**, *34*, 3909−3917.

(28) Vasudevan, S. A.; Rauh, A.; Barbera, L.; Karg, M.; Isa, L. Stable in Bulk and Aggregating at the Interface: Comparing Core-Shell Nanoparticles in Suspension and at Fluid Interfaces. *Langmuir* **2018**, *34*, 886−895.

(29) Scotti, A.; Bochenek, S.; Brugnoni, M.; Fernandez-Rodriguez, M. A.; Schulte, M. F.; Houston, J. E.; Gelissen, A. P. H.; Potemkin, I. I.; Isa, L.; Richtering, W. Exploring the colloid-to-polymer transition for ultra-low crosslinked microgels from three to two dimensions. *Nat. Commun.* **2019**, *10*, No. 1418.

(30) Vogel, N.; Fernández-López, C.; Pérez-Juste, J.; Liz-Marzán, L. M.; Landfester, K.; Weiss, C. K. Ordered Arrays of Gold Nanostructures from Interfacially Assembled Au@PNIPAM Hybrid Nanoparticles. *Langmuir* **2012**, *28*, 8985−8993.

(31) Bochenek, S.; Scotti, A.; Ogieglo, W.; Fernández-Rodríguez, M. A.; Schulte, M. F.; Gumerov, R. A.; Bushuev, N. V.; Potemkin, I. I.; Wessling, M.; Isa, L.; Richtering, W. Effect of the 3D Swelling of Microgels on Their 2D Phase Behavior at the Liquid-Liquid Interface. *Langmuir* **2019**, *35*, 16780−16792.

(32) Bolhuis, P.; Frenkel, D. Isostructural solid-solid transitions in systems with a repulsive 'shoulder' potential. *J. Phys.: Condens. Matter* **1997**, *9*, 381−387.

(33) Denton, A. R.; Löwen, H. Isostructural solid-solid transitions in square shoulder systems. *J. Phys.: Condens. Matter* **1997**, *9*, L1−L5.

(34) Hemmer, P. C.; Velasco, E.; Mederos, L.; Navascués, G.; Stell, G. Solid-solid transitions induced by repulsive interactions. *J. Chem. Phys.* **2001**, *114*, 2268−2275.

(35) Navascués, G.; Velasco, E.; Mederos, L. Solid−solid transitions induced by repulsive interactions revisited. *J. Phys.: Condens. Matter* **2016**, *28*, No. 414002.

(36) Jagla, E. A. Phase behavior of a system of particles with core collapse. *Phys. Rev. E* **1998**, *58*, 1478−1486.

(37) Glaser, M. A.; Grason, G. M.; Kamien, R. D.; Košmrlj, A.; Santangelo, C. D.; Ziherl, P. Soft spheres make more mesophases. *Europhys. Lett.* **2007**, *78*, No. 46004.

(38) Du, Y.; Jiang, H.; Hou, Z. Self-assembly of active core corona particles into highly ordered and self-healing structures. *J. Chem. Phys.* **2019**, *151*, No. 154904.

(39) Somerville, W. R. C.; Law, A. D.; Rey, M.; Vogel, N.; Archer, A. J.; Buzza, D. M. A. Pattern formation in two-dimensional hard-core/soft-shell systems with variable soft shell profiles. *Soft Matter* **2020**, *16*, 3564−3573.

(40) Malescio, G.; Pellicane, G. Stripe phases from isotropic repulsive interactions. *Nat. Mater.* **2003**, *2*, 97−100.

(41) Fornleitner, J.; Kahl, G. Pattern formation in two-dimensional square-shoulder systems. *J. Phys.: Condens. Matter* **2010**, *22*, No. 104118.

(42) Pattabhiraman, H.; Dijkstra, M. On the formation of stripe, sigma, and honeycomb phases in a core-corona system. *Soft Matter* **2017**, *13*, 4418−4432.

(43) Dotera, T.; Oshiro, T.; Ziherl, P. Mosaic two-lengthscale quasicrystals. *Nature* **2014**, *506*, 208−211.

(44) Jagla, E. A. Core-softened potentials and the anomalous properties of water. *J. Chem. Phys.* **1999**, *111*, 8980−8986.

(45) Jagla, E. A. Minimum energy configurations of repelling particles in two dimensions. *J. Chem. Phys.* **1999**, *110*, 451−456.

(46) Pelton, R. Temperature-Sensitive Aqueous Microgels. *Adv. Colloid Interface Sci.* **2000**, *85*, 1−33.

(47) Kröger, L. C.; Kopp, W. A.; Leonhard, K. Prediction of Chain Propagation Rate Constants of Polymerization Reactions in Aqueous NIPAM/BIS and VCL/BIS Systems. *J. Phys. Chem. B* **2017**, *121*, 2887−2895.

(48) Wu, X.; Pelton, R. H.; Hamielec, A. E.; Woods, D. R.; McPhee, W. The kinetics of poly(N-isopropylacrylamide) microgel latex formation. *Colloid Polym. Sci.* **1994**, *272*, 467−477.

(49) Fernández-Barbero, A.; Fernández-Nieves, A.; Grillo, I.; López-Cabarcos, E. Structural modifications in the swelling of inhomogeneous microgels by light and neutron scattering. *Phys. Rev. E* **2002**, *66*, No. 051803.

(50) Still, T.; Chen, K.; Alsayed, A. M.; Aptowicz, K. B.; Yodh, A. G. Synthesis of micrometer-size poly(N-isopropylacrylamide) microgel particles with homogeneous crosslinker density and diameter control. *J. Colloid Interface Sci.* **2013**, *405*, 96−102.

(51) Kyrey, T.; Witte, J.; Feoktystov, A.; Pipich, V.; Wu, B.; Pasini, S.; et al. Inner structure and dynamics of microgels with low and medium crosslinker content prepared via surfactant-free precipitation polymerization and. *Soft Matter* **2019**, *15*, 6536−6546.

(52) Rey, M.; Uttinger, M. J.; Peukert, W.; Walter, J.; Vogel, N. Probing particle heteroaggregation using analytical centrifugation. *Soft Matter* **2020**, *16*, 3407−3415.

(53) Fernandez-Rodriguez, M. A.; Antonopoulou, M.-N.; Isa, L. Near-zero surface pressure assembly of rectangular lattices of microgels at fluid interfaces for colloidal lithography. *Soft Matter* **2021**, *17*, 335−340.

(54) Harrer, J.; Rey, M.; Ciarella, S.; Löwen, H.; Janssen, L. M. C.; Vogel, N. Stimuli-Responsive Behavior of PNiPAm Microgels under Interfacial Confinement. *Langmuir* **2019**, *35*, 10512−10521.

(55) Kolker, J.; Harrer, J.; Ciarella, S.; Rey, M.; Ickler, M.; Janssen, L. M. C.; Vogel, N.; Löwen, H. Interface-Induced Hysteretic Volume Phase Transition of Microgels: Simulation and Experiment. 2021, arXiv:2102.01536. arXiv.org e-Print archive. https://arxiv.org/abs/2102.01536.

(56) Ninarello, A.; Crassous, J. J.; Paloli, D.; Camerin, F.; Gnan, N.; Rovigatti, L.; Schurtenberger, P.; Zaccarelli, E. Modeling microgels with a controlled structure across the volume phase transition. *Macromolecules* **2019**, *52*, 7584−7592.

(57) Rovigatti, L.; Gnan, N.; Ninarello, A.; Zaccarelli, E. Connecting Elasticity and Effective Interactions of Neutral Microgels: The Validity of the Hertzian Model. *Macromolecules* **2019**, *52*, 4895−4906.

(58) Rovigatti, L.; Gnan, N.; Zaccarelli, E. Internal structure and swelling behaviour of in silico microgel particles. *J. Phys.: Condens. Matter* **2017**, *30*, No. 044001.

(59) Gnan, N.; Rovigatti, L.; Bergman, M.; Zaccarelli, E. In Silico Synthesis of Microgel Particles. *Macromolecules* **2017**, *50*, 8777−8786.

(60) Choudhury, C. K.; Palkar, V.; Kuksenok, O. Computational Design of Nanostructured Soft Interfaces: Focus on Shape Changes and Spreading of Cubic Nanogels. *Langmuir* **2020**, *36*, 7109−7123.

(61) Bushuev, N. V.; Gumerov, R. A.; Bochenek, S.; Pich, A.; Richtering, W.; Potemkin, I. I. Compression and Ordering of Microgels in Monolayers Formed at Liquid−Liquid Interfaces: Computer Simulation Studies. *ACS Appl. Mater. Interfaces* **2020**, *12*, 19903−19915.

(62) Brito, C.; Lerner, E.; Wyart, M. Theory for Swap Acceleration near the Glass and Jamming Transitions. *Phys. Rev. X* **2018**, *8*, 1−12.

(63) Kapteijns, G.; Ji, W.; Brito, C.; Wyart, M.; Lerner, E. Fast generation of ultrastable computer glasses by minimization of an augmented potential energy. *Phys. Rev. E* **2019**, *99*, No. 012106.

(64) Stillinger, F. H.; Weber, T. A. Computer simulation of local order in condensed phases of silicon. *Phys. Rev. B* **1985**, *31*, 5262−5271.

(65) Tersoff, J. Modeling solid-state chemistry: Interatomic potentials for multicomponent systems. *Phys. Rev. B* **1989**, *39*, 5566−5568.

(66) Löwen, H.; Allahyarov, E. Role of effective triplet interactions in charged colloidal suspensions. *J. Phys.: Condens. Matter* **1998**, *10*, 4147−4160.

(67) Brenner, D. W.; Shenderova, O. A.; Harrison, J. A.; Stuart, S. J.; Ni, B.; Sinnott, S. B. A second-generation reactive empirical bond order (REBO) potential energy expression for hydrocarbons. *J. Phys.: Condens. Matter* **2002**, *14*, 783−802.

(68) Ciarella, S.; Sciortino, F.; Ellenbroek, W. G. Dynamics of Vitrimers: Defects as a Highway to Stress Relaxation. *Phys. Rev. Lett.* **2018**, *121*, No. 058003.

(69) Kob, W.; Andersen, H. C. Scaling behavior in the β-relaxation regime of a supercooled Lennard-Jones mixture. *Phys. Rev. Lett.* **1994**, *73*, 1376−1379.

(70) Harrer, J.; Ciarella, S.; Rey, M.; Löwen, H.; Janssen, L. M. C.; Vogel, N. Collapse-induced phase transitions in binary interfacial microgel monolayers. *Soft Matter* **2021**, DOI: 10.1039/D1SM00318F.

(71) Rey, M.; Law, A. D.; Buzza, D. M. A.; Vogel, N. Anisotropic Self-Assembly from Isotropic Colloidal Building Blocks. *J. Am. Chem. Soc.* **2017**, *139*, 17464−17473.

(72) Camerin, F.; Gnan, N.; Ruiz-Franco, J.; Ninarello, A.; Rovigatti, L.; Zaccarelli, E. Microgels at Interfaces Behave as 2D Elastic Particles Featuring Reentrant Dynamics. *Phys. Rev. X* **2020**, *10*, No. 031012.

(73) Rey, M.; Yu, T.; Guenther, R.; Bley, K.; Vogel, N. A dirty story: Improving colloidal monolayer formation by understanding the effect of impurities at the air/water interface. *Langmuir* **2019**, *35*, 95−103.

(74) Rey, M.; Yu, T.; Bley, K.; Landfester, K.; Buzza, D. M. A.; Vogel, N. Amphiphile-Induced Anisotropic Colloidal Self-Assembly. *Langmuir* **2018**, *34*, 9990−10000.

(75) Ciach, A.; Pękalski, J. Exactly solvable model for self-assembly of hard core−soft shell particles at interfaces. *Soft Matter* **2017**, *13*, 2603−2608.

(76) Frenkel, D.; Smit, B. In *Physics Today*; Frenkel, D.; Smit, B., Eds.; Academic Press: San Diego, 2002; Vol. *50*, p 638.

(77) Weeks, J. D.; Chandler, D.; Andersen, H. C. Role of Repulsive Forces in Determining the Equilibrium Structure of Simple Liquids. *J. Chem. Phys.* **1971**, *54*, 5237−5247.

(78) Dijkstra, M.; Brader, J. M.; Evans, R. Phase behaviour and structure of model colloid-polymer mixtures. *J. Phys.: Condens. Matter* **1999**, *11*, 10079−10106.

(79) Berthier, L.; Flenner, E.; Fullerton, C. J.; Scalliet, C.; Singh, M. Efficient swap algorithms for molecular dynamics simulations of equilibrium supercooled liquids. *J. Stat. Mech.: Theory Exp.* **2019**, *2019*, No. 064004.

(80) Likos, C. N.; Blaak, R.; Wynveen, A. Computer simulations of polyelectrolyte stars and brushes. *J. Phys.: Condens. Matter* **2008**, *20*, No. 494221.

(81) Louis, A. A. Beware of density dependent pair potentials. *J. Phys.: Condens. Matter* **2002**, *14*, 9187−9206.

(82) Senff, H.; Richtering, W. Temperature sensitive microgel suspensions: Colloidal phase behavior and rheology of soft spheres. *J. Chem. Phys.* **1999**, *111*, 1705−1711.

(83) Lin, Y.-C.; Rotenberg, B.; Dzubiella, J. Structure and position-dependent properties of inhomogeneous suspensions of responsive colloids. *Phys. Rev. E* **2020**, *102*, No. 042602.

(84) Baul, U.; Dzubiella, J. Structure and dynamics of responsive colloids with dynamical polydispersity. *J. Phys.: Condens. Matter* **2021**, *33*, 174002.

(85) Berendsen, H. J. C.; Postma, J. P. M.; van Gunsteren, W. F.; DiNola, A.; Haak, J. R. Molecular dynamics with coupling to an external bath. *J. Chem. Phys.* **1984**, *81*, 3684−3690.

(86) Bitzek, E.; Koskinen, P.; Gähler, F.; Moseler, M.; Gumbsch, P. Structural Relaxation Made Simple. *Phys. Rev. Lett.* **2006**, *97*, No. 170201.